The Beauty of Less Perfect Light: A High Resolution Interferometer for Characterizing Broadband Light Sources

Intel Science Talent Search
November 2004

Jonathan Wu

Great Neck South High School
Great Neck, New York

and

Laser Teaching Center
Stony Brook University

1 Introduction

Laser light has largely been favored over incoherent light due to its practicality in experiments, technology, and even everyday life (laser printers and pointers). It is characterized by a high degree of spatial and temporal coherence, measures of light's ability to maintain phase relationships. Spatial coherence describes wavefronts of light originating from or able to be focused to a point, while temporal coherence, the measurement of phase correlation of light or the ability of light to stay "in step" over long distances, conveys the monochromaticity of a source.[1]

Despite the versatility of laser light and its ability to maintain phase stability, there are certain applications in which less than perfect light is not only a substitute for laser light but is an essential ingredient. Optical coherence tomography (OCT), a method for imaging inside turbid media, such as living tissue, is one such application.[2] In OCT the short coherence length of a broadband light source (typically on the scale of microns) is used to identify or select the depth from which photons have scattered. By scanning in a depth direction z and two transverse axes x and y, optical coherence setups can image slices of tissue gathered in the $x - y$ plane and piece together three dimensional maps of tissue by layering the 2-D images on one another.[3] Currently OCT is used as a diagnostic technique for imaging the eye, which is mostly transparent. However, OCT's real potential lies in the possibility for identifying tumors in tissue and replacing conventional invasive biopsy.[4] OCT instruments are not commercially available, but a number of medical physics research groups have built systems from widely available components. The OCT device at Harvey Mudd College was developed largely by undergraduate students, and has been used for a variety of studies on frog embryos and plants.[3] In addition, a biomedical engineering group at Stony Brook University is developing a miniaturized device that could be used in hospitals for *in situ* bladder cancer detection.[5] Both instruments are based on fiber optics, the benefits of which are discussed in later sections.

In order to characterize light sources used in OCT, a simple but highly effective scanning Michelson interferometer was developed and used to study the coherence properties of several broadband light sources and to demonstrate the physical principle of depth selection. Two distinct mechanisms for controlling the motion of the interferometer's scanning mirror were implemented. Both used a 1.8 degree per step stepping motor for movement. The first of these, whose active component is an ordinary rubber band, can translate a mirror in 1.2

nanometer (nm) steps over a range of up to 12.7 microns (μm). The second mechanism, which is based on a long lever, covers a range of up to 0.2 millimeter (mm) with a lower resolution of about 45.2 nm per step. Each translation scheme had its own uses in exploring various light sources, including a helium-neon (He-Ne) laser, filtered and unfiltered halogen-bulb white light, and light-emitting diodes (LEDs). The eventual goal of this project is to develop a similar OCT system by first investigating the attributes of broadband, incoherent light sources and establishing new approaches to problems which plague modest, open-air OCT instruments such as alignment and signal detection.

2 Optical Coherence Tomography

Although it has only been a decade since the publication of the first paper on OCT techniques by D. Huang *et. al.* in 1991, optical coherence tomography has received an enthusiastic response in the fields of biomedical engineering and physical optics for its precise cross-sectional tomographic imaging capabilities.[2] The successes of *in vivo* OCT tissue imaging have been stressed primarily because of the many limiting factors of flesh in obstructing other imaging devices, such as high-frequency ultrasound.[6] The low resolution of ultrasound makes it unfeasible for use in identifying minute yet critical abnormalities in tissue such as cancerous malignancies. On the other hand, OCT is rising as an improved substitute for biopsies and otherwise invasive diagnostic techniques in sensitive tissues like those in the retina or brain.[4][7] Optical coherence microscopes and tomography devices continue to be constructed in the likeness of the original design, which was based centrally around a Michelson interferometer. Figure 1 shows a typical OCT setup.

Usage of interferometry in OCT is what allows for analysis of tissue structures from various depths. Most systems currently in development are built using optical fiber components, due to various complications inherent in an open-air system, such as ambient light and difficult alignment.[2][5][7] To examine the tissue sample, a broadband light source is fed into an optical fiber, and a fiber coupler separates the light into two "arms," the sample arm and the reference arm. The reference arm is the mobile mirror in the Michelson, whereas the sample arm points to the tissue itself.[2] For any amount of light that enters tissue, however, the great majority scatters, as evidenced by the red glowing of your finger when a laser is shined through it. Only some light scatters directly back from the sample.[4] In order for interference to occur, the path difference between light traveling to the sample arm and light

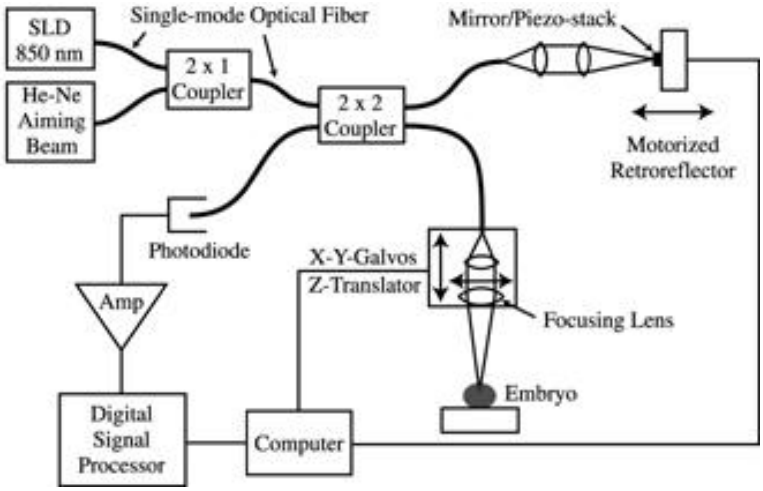

Figure 1: A typical optical coherence tomography setup. [3]

traveling to the reference arm must be smaller than the coherence length of the light (~ 10 microns for typical OCT light sources). Thus, only light returning from a depth equal to the length of the reference arm will register a signal, allowing for precise scanning of narrow depths in tissue. To check for signal, the reference arm is vibrated using a piezo-electric transducer (PZT).[8] Due to the vibrating reference arm, the interference that is detected by the photodetector will change in intensity, resulting in an AC electrical signal. Depending on the scattering and absorption rates of the specific area of tissue, the AC signal will vary. Demodulation of the signal reveals the composition of the tissue. Through lateral scanning with directional mirrors, a 2-D image can be obtained froma specific scanning depth, and by layering images from different depths a three-dimensional map is resolved.[3]

To obtain sharp resolution, high bandwidth sources such as superluminescent diodes (SLDs) and titanium-sapphhire (Ti-Sapph) lasers are used. SLDs, bright, directional, spontaneous emission light sources akin to common LEDs (light-emitting diodes) are currently the most popular.[9] Due to the low coherence of these sources, light returning from only a small range of depths close to the length of the OCT reference arm will produce a signal. Some groups have achieved spatial resolution of 6 microns, the size of individual cells, using SLDs.[5] In order to better understand the concepts of OCT, however, it is necessary to examine the original interferometer, basic interferometric principles, and how they apply to modern OCT tecniques.

3 Interferometer Theory

3.1 Michelson's Device

In 1887, Albert A. Michelson, the inventor of the interferometer that now bears his name, cooperated with Edward Morley to design an experiment to ascertain the existence of ether in space. Their instrument consisting of two mirrors orthogonal to one another, a beam splitter (or a half-silvered glass plate) at a 45° angle to each of these mirrors, and a light source (see Figure 2 for a schematic of a typical Michelson interferometer).[10] Though the Michelson interferometer was used to prove that ether was non-existent, the instrument today has a greatly different role in creating tomographic images of tissue. The interferometer works by splitting incoming light into two beams each with half the intensity of the original, traveling on two different, orthogonal optical paths. When the two beams reflect off their respective mirrors and recombine at the beam splitter, they interfere, producing an interference pattern.[11] However, this only occurs if the length difference between the two paths is shorter than the coherence length of the light source.

3.2 Fourier Transform Spectroscopy

The most explored, well-established, and efficient method of determining various frequencies present in a single source of light is Fourier transform spectroscopy (FTS). Though theoretically in existence since Michelson's time, FTS was applied to spectral analysis only starting in the mid-20th century. At this point, the advent of viable computer algorithms required to carry out mathematical Fourier analysis turned FTS into something that could be performed at a well-endowed undergraduate laboratory.[12][13]

Unlike traditional slit and grating spectrometers, which rely on the narrowness of a physical slit and use of a diffraction grating to resolve a broadband source into its various components, Fourier transform spectrometers are based on the Michelson interferometer.[13] By directing light through a Michelson, translating one mirror arm mirror, and recording the change in intensity of the interference pattern, an interferogram can be formed—a correlation between interference intensity and path length difference.[10] Using a Fourier transform algorithm, defined by

$$S(k) = \frac{2}{\pi} \int_0^\infty R(\Delta)\phi(\Delta)\cos(k\Delta)d\Delta, \tag{1}$$

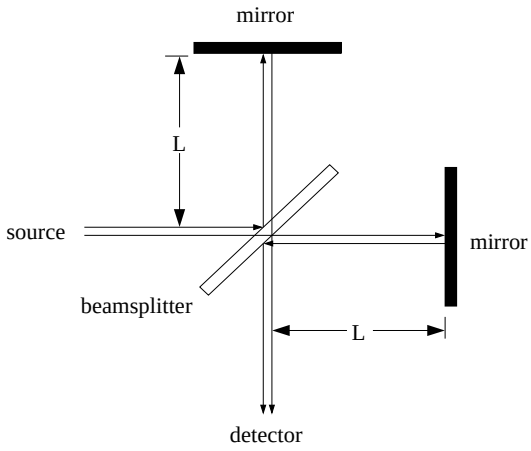

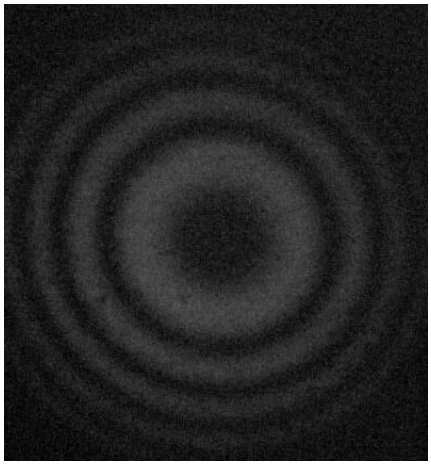

Figure 2: Diagram of a Michelson interferometer (left), and bullseye interference (right).

where $S(k)$ is the spectrum function, $R\Delta$ is a square function defining the limits of the Fourier transform spectrometer (since the path length cannot reach an infinite distance), $\phi\Delta$ is the interferogram function (usually a sine wave or combination of sine waves), and $k = \frac{2\pi}{\lambda}$ where λ is the wavelength of the light.[13] By transforming an interferogram using this equation, a standard frequency-intensity graph can be derived.[14] From the spikes and distribution of such a graph, the spectral composition, the frequencies of light present and dominant in the source, is shown. Using concepts present in FTS, such as interferogram scanning and resolution of frequency distribution from interferograms, it is much easier to see the relationship between coherence length and bandwidth.

3.3 Coherence and Spectral Distribution

The coherence properties of a light source depend solely on the light source's spectral composition. A truly monochromatic or temporally coherent wave would have an infinitely long coherence length. However, because monochromatic point sources of light are unattainable, for all sources coherence length is a specific value, determined by the bandwidth, or wavelength distribution, of light. Because any source of electromagnetic radiation has a finite bandwidth represented by a spread of wavelengths $\lambda \pm \Delta\lambda$, and the waves that compose the light source must at some point constructively interfere, light waves must also at some point destructively interfere [1]. The distance between these two interactions is known as the coherence length, represented by

$$l_c = \frac{\lambda^2}{2\pi\Delta\lambda}. \tag{2}$$

From this, it is evident that wider bandwidths or spectral distributions directly correspond to shorter coherence lengths. The inverse relationship between coherence length and spectral width is illustrated by the superimposition of sine curves with different frequencies shown in Figure 3. In the top figure the wavelengths or frequencies differ by 10%, and there are about 10 waves per period of the combined waveform. In the next figure the frequency separation is reduced to 5%, and there are about 20 waves per period. In the final figure, eleven frequencies are present over a frequency range of 10%. This produces a non-periodic waveform in which all lobes except the central peak are suppressed.

4 Experimental Apparatus and Setup

The major components of the setup were: the beam splitter and mirrors comprising the interferometer; two different motion-control devices for translating one of the mirrors in submicron steps; various light sources; and a photodetector and data recording device. The components were mounted on a standard optical table. Both motion-control devices utilized a standard low-resolution translation stage with a range of 1.0 inch moved by a micrometer calibrated in steps of 0.001 inch. The stage was driven by a standard 200 step per revolution stepper motor coupled to the micrometer shaft with a short length of thick rubber tubing. The tubing was flexible enough to accomodate for a 1 cm height difference in the motor and micrometer shafts. Two types of motion control devices were needed because there is

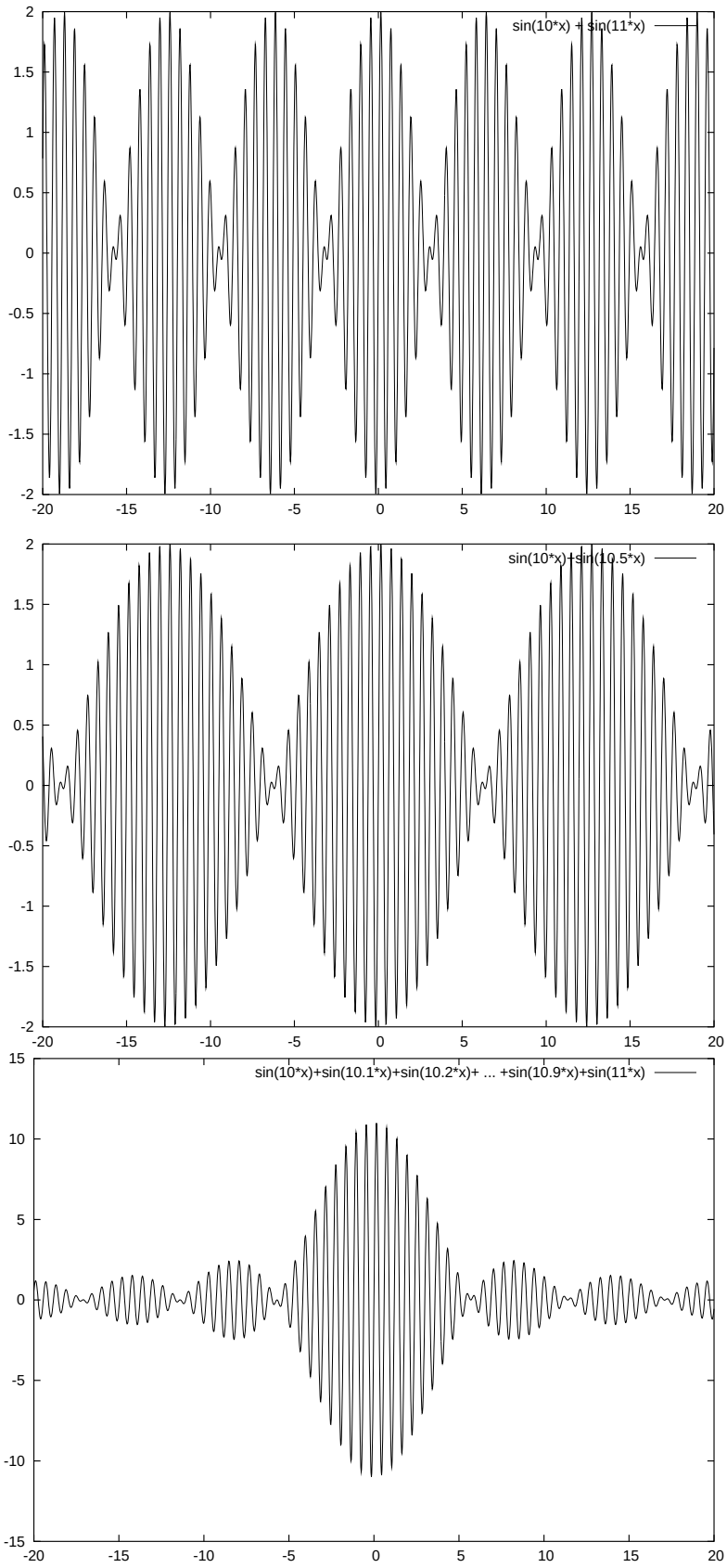

Figure 3: Examples of superimposed sine waves of varying frequencies.

inevitably a trade-off between resolution and scanning range; it is simply not possible to accurately move a mirror a long distance in precise, minute steps without a feedback system such as a complementary He-Ne laser to measure exactly how far the mirror is moving.

4.1 Interferometer Setup

An anti-reflection coated 20 mm cube type beam splitter with a 50–50 transmission-reflectance ratio was used for the interferometer. The two 5 cm square gold-coated first surface mirrors were mounted ∼5 cm from adjacent faces of the cube. The mirrors were attached with foam-type double-surface mounting tape, which provided surprising stability, on Thorlabs KM-1 mirror mounts. For the He-Ne trial only, a 50 μm diameter pinhole was placed in front of the laser to diffract the light into the interferometer. Thorlabs TR series posts and PH series post holders were used to secure all components ∼11 cm above the optical table.

Before mounting the photodetector, the interference pattern was projected onto a viewing screen. For the He-Ne trials only, the image was expanded by placing a 10x microscope objective 2.5 cm away from the beamsplitter. The objective also served to eliminate the unwanted outer portions of the Airy diffraction pattern created by the pinhole. The fringes were centered around the bullseye pattern by adjusting the mirrors until the center of circular fringes appeared.

4.2 Motion Control - High Resolution

A modest method was found to translate the interferometer mirror effectively over a limited range of a few microns in minute steps on the order of nanometers. Either one or two rubber bands were used to pull on the mirror mount using the translator, as shown in Figure 4; the use of two rubber bands allowed for increased range (due to the increased applied force) with reduced resolution. The imperceptible deformation of the mirror mount due to the force exerted by the rubber band was as small as 1.2 nm with one rubber band, a figure calculated from the measurement of He-Ne laser fringes to be described later. Piezo-electric transducer (PZT) devices used in commercial and research scanning spectrometers have similar range and resolution, but are obviously much more complex and expensive.

Figure 5 shows the relationship between the response of the rubber band to changing load. In the experiment the length of the rubber band was between 16 and 18.5 cm, and over this range the change in force is nearly proportional to the change in length.

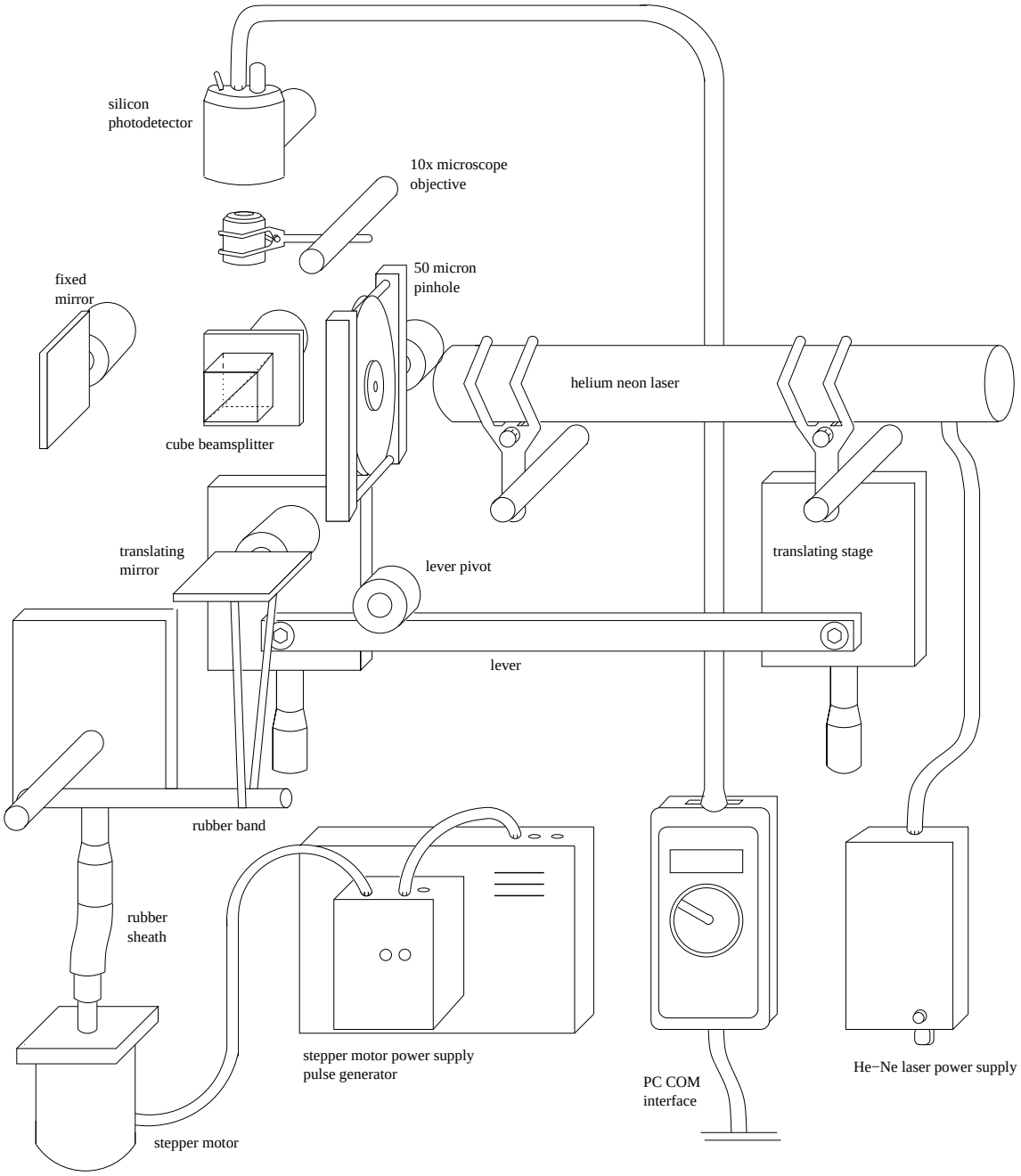

Figure 4: Diagram of the experimental setup.

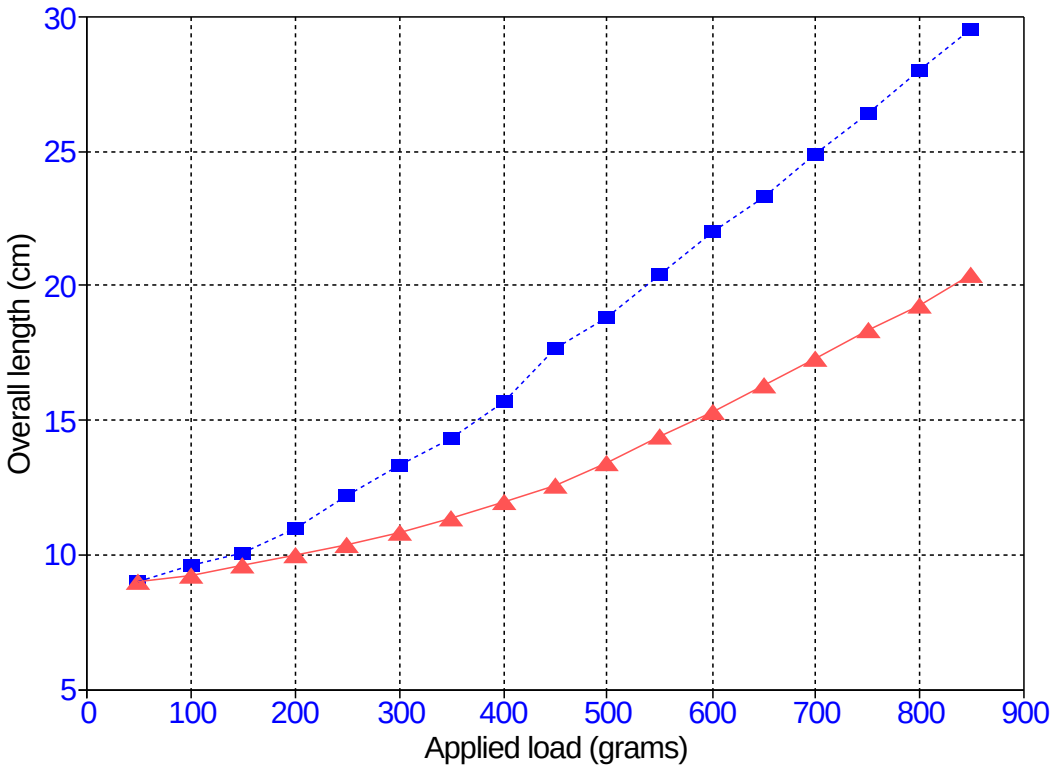

Figure 5: Rubber band response to applied load for single (squares) and dual bands (triangles).

To determine the effectiveness of the rubber band as a translator, simple measurements were conducted to determine the proportionality constant between the movements and the subsequent path length difference in the Michelson. The equations

$$\Delta L = f\frac{\lambda}{2} \tag{3}$$

and

$$\Delta L = kn, \tag{4}$$

where ΔL is the path length difference, λ is the wavelength of the light, and f is the number of interference fringes scanned, were manipulated to determine k, the distance traveled per step of the motor.[13] Translating the stage a number of steps n, and determining using collected data the number of interference fringes f that pass by (the shift of interference intensity at a specific point shifting from dark to light to dark again denotes one cycle) allows solving for k by setting

$$\frac{f\lambda}{2} = kn. \tag{5}$$

By taking a sample from single-rubber band He-Ne intensity data of 13 interference fringes comprised of 3454 data points at $\lambda = 632.8$ nm, k is calculated to be 1.19 nanometers per step. Unfortunately, high resolution comes at the cost of scanning range, which is limited by the micrometer's one inch travel. At the greatest extent of the translator's range, only twenty He-Ne fringes can be resolved with the apparatus, meaning range is limited to a mere 6.3 microns. Data taken from a dual rubber band trial yields 10 fringes comprised of 941 data points; k is calculated to be 3.36 nm, at a maximum range of 6.33 microns.

4.3 Motion Control - Medium Resolution

The necessarily limited range of the rubber band system makes scanning over the entire coherence length of a broadband source difficult without taking small pieces of data and then linking them together by hand. Therefore, a coarser scanning mechanism with longer range – based on the use of a 61 cm long section of optical rail acting as a lever – was created. As shown in Figure 4, two spring-loaded translation stages were bolted parallel to each other with an optical post holder bolted in between; the post holder held a small arm, the tip of which served as the pivot of the lever. The lever was set up so that the portion from the pivot to the active translator was 50.7 cm, while the length from the pivot to the translation stage being driven was 0.9 cm. The active translator was driven by the standard stepper motor described previously. Data taken with the He-Ne yielded 3859 data points covering 551 fringes, and thus a step size of 45.2 nm. The maximum range was somewhat greater: 605 fringes or 0.19 mm.

4.4 Light sources

The first light source employed was a standard 10 mW red (632.8 nm) He-Ne laser. The laser beam was directed into a 50μm diameter pinhole that diffracted the emerging light into an Airy pattern that had a convenient divergence and uniform wavefronts. The laser light was used mainly for alignment, testing, and calibration. Its high monochromaticity and coherence length of 30 cm or more resulted in no change in the visibility of the interference fringes observed in this experiment.

A sodium gas lamp was then obtained and used to observe the periodic "beating" of the fringe pattern that occurs when a light source has two distinct closely-spaced spectral lines. The fringe patterns were observed by viewing the image of the lamp through the interferometer, rather than by projecting the fringes on to a screen.

The next light source used was a moderately broadband red light with an average wavelength close to that of a He-Ne laser, and was a good representation of broad band sources used in OCT. It was created by directing bright white light from a halogen lamp through a fiber optic bundle on to a Melles Griot 03 FIL 224 interference filter with a bandwidth of 10.58 nm (see Figure 6). In order to reach near-zero path length difference, the only range in which broadband light can interfere, the physical separation of each mirror from the beam-splitter cube was first set to be as nearly equal as possible. Starting from this point the elastic band and lever methods were used to find the exact position of zero path length difference.

Finally, white light fringes were visually observed by removing the red interference filter, and green light fringes were observed using a LED as the source. An LED was used because superluminescent diodes, broadband sources closely related to LEDs, are widely used in current OCT systems.

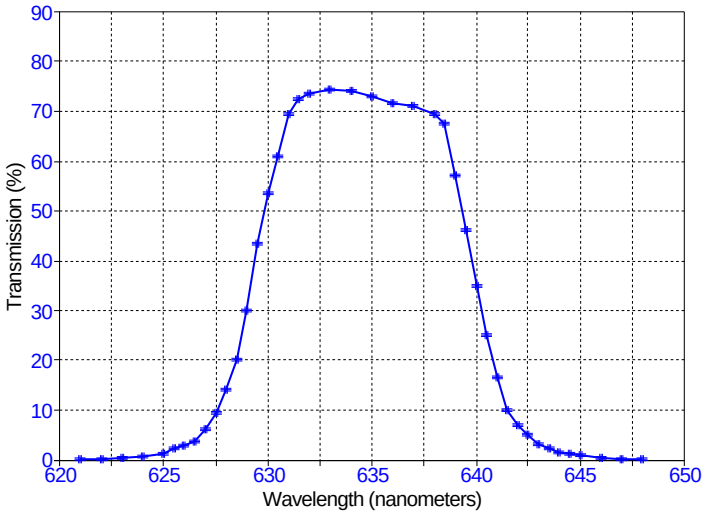

Parameter	Value
Part number	03 FIL 224
Center wavelength	634.62 nm
50% bandwidth	10.58 nm
10% bandwidth	14.66 nm
1% bandwidth	21.27 nm
Peak transmission	74.3%

Figure 6: Transmission curve (left) and other specifications(right) of the red light filter.

4.5 Data Collection

Changing fringe patterns were recorded with a Thorlabs DET-110 photodector sheathed in paper to lessen the effects of ambient lighting on measurements. The output was digitized with a RadioShack Model 22-812 digital multimeter interfaced to a Windows PC. A 100 kΩ resistor was typically used to convert the current signal from the detector into an average voltage of about 50 mV (with the He-Ne a 30 kΩ resistor was used to create readings between 1 and 28 mV). The MeterView software that came with the meter stored one reading per second at its fastest collection rate in a data file. The data file could later be imported into a spreadsheet program for analysis and plotting. A pulse generator was used to drive the stepper motor as the software recorded intensity readings from the photodetector.

5 Results and Analysis

5.1 He-Ne Laser Light

The sequence of He-Ne fringes shown in Figure 7 was taken at a 500 ms pulse spacing with the single-rubber-band system. These data were used to determine the mirror movement per step, as described previously in Section 4.2. The amplitude or visibility of the fringes remains constant across the entire plot, as expected, since the coherence length of the He-Ne laser is much longer than the scanning range of $\sim 5\mu$m.

5.2 Sodium Lamp Light

The yellow sodium fringes periodically changed in visibility as the mirror was directly (without any lever) translated with the micrometer, as predicted by the top two plots in Figure 3. The distance between successive maxima or minima of fringe visibility was found to be 11.0 mils (thousandths of an inch), or 279 μm. The separation of the two spectral lines can be obtained from these data with the help of the following formula:

$$\Delta\lambda = \frac{\lambda^2}{2(\Delta d)} \tag{6}$$

where Δd is the movement of the mirror, $\lambda = 589$ nm is the average wavelength of the two lines, and $\Delta\lambda$ is their wavelegth separation [15]. The result is $\Delta\lambda = 0.62$ nm, in very good agreement with the known value 589.592 - 588.995 = 0.597 nm.[16]

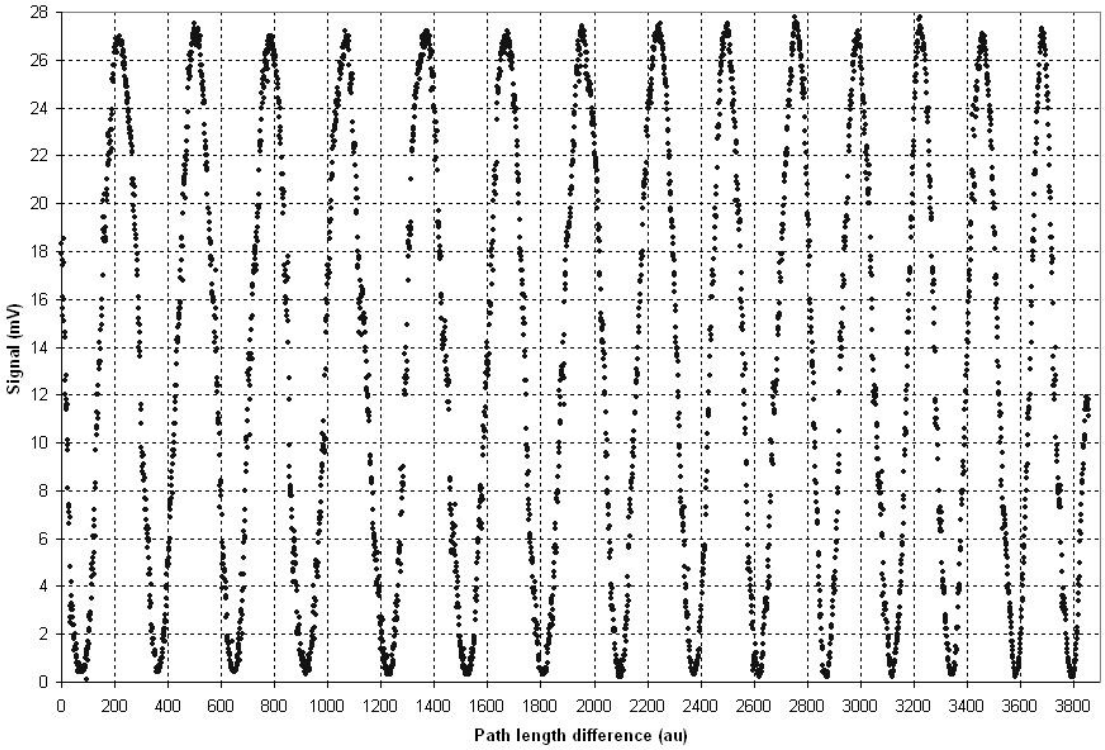

Figure 7: He-Ne interferogram scan taken at 500 ms pulse spacing.

In addition, it was observed that maximum fringe visibility gradually diminished as the micrometer reached the end of its range. (Path length difference $\geq$ 1 cm). This effect is most likely due to the non-zero spectral width of each of the two sodium lines.

5.3 Filtered White Light

The range of the rubber band was so limited that in order to scan the entire central visibility lobe of the filtered red light interferogram, the lever system had to be used. At near-zero path length, the visibility of the interference pattern, represented by

$$V = \frac{(I_{\max} - I_{\min})}{(I_{\max} + I_{\min})}, \tag{7}$$

V representing visibility and I light intensity, is the greatest.[13] As the system translates away from zero path length, interference intensity drops and does not return to its maximum intensity. This result is consistent with the predicted visibility pattern of a broadband source with many frequencies or wavelengths in the last illustration of Figure 3.

Additionally, the fringe envelope encompassing the fringe pattern can be analyzed to determine the bandwidth of the source being examined. Although a Fourier transform was

not performed, an approximate determination of the red light filter's bandwidth can be ascertained using visibility readings. To determine the fringe visibility pattern, a Gaussian envelope function of the form

$$I_{\max/\min} = (c_1 + c_2 n) \pm c_3 e^{-\frac{(n-c_4)^2}{w^2}} \tag{8}$$

Here, n is the data point (step) number; $I_{\max}$ and $I_{\min}$ correspond to the maximum and minimum intensities at a given point in the fringe pattern; $I_{\max}$ corresponds to the plus sign and $I_{\min}$ corresponds to the minus sign in the equation. $c_1 + c_2 n$ is a linear function which describes the background level in the absence of fringes; c_3 is the amplitude of the Gaussian envelope; c_4 is the center data point of the envelope; and w is the width parameter of the Gaussian.[15] The appropriate values of the adjustable parameters of the equation were determined by visually matching the envelope function to the recorded data, as shown in Figure 8. The width w obtained from matching the envelope to the data was 240 steps with an uncertainty of ± 20 steps.

A more appropriate measure than w for describing the width of the Gaussian envelope is the full width half maximum (FWHM), which is defined by this formula [15]:

$$FWHM = 2w\sqrt{-ln(\frac{1}{2})} = 1.66w = 397 \text{ steps.} \tag{9}$$

The *physical distance* Δd corresponding to FWHM = 397 steps is given by

$$\Delta d = w\frac{\lambda}{2n_{\mathrm{f}}} \tag{10}$$

where $2n_{\mathrm{f}}$ is the number of points per fringe (7 points per fringe was the resolution of the lever system).[15] The result is $\Delta d = 18.1 \pm 1.5\ \mu m$.

It is now possible to estimate the spectral width of the red light source by employing Equation 6 previously applied to the sodium doublet. The result is $\Delta\lambda = 11.1 \pm 1$ nm. This number compares very favorably with the spectral FWHM of 10.58 nm provided by the manufacturer of the filter (see Figure 6).

5.4 Other Light Sources

Visual observations were made with both LEDs and the unfiltered white light halogen source. The white light fringes were viewed first, as it was convenient to simply take out the red light

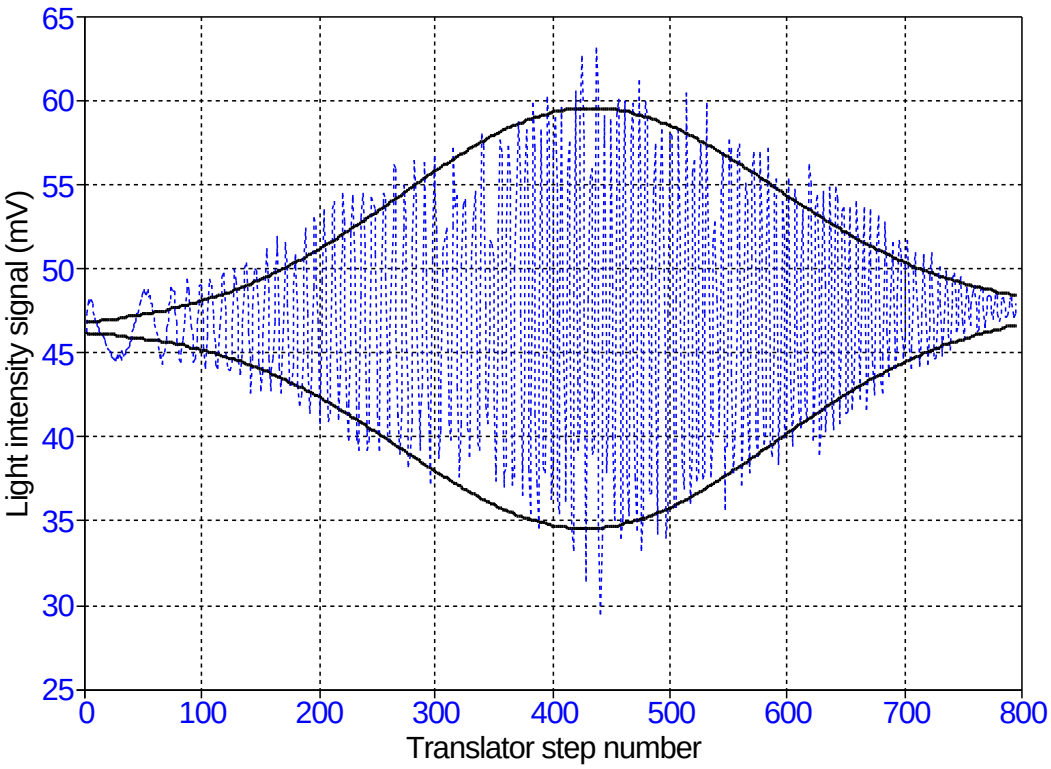

Figure 8: The red light interferogram with a fitted theoretical visibility envelope.

filter when the fringe visibility of the filtered light was at its maximum (when path length difference was near zero). The interference of the white light entering the interferometer was scanned by pulling on the rubber band. Similarly, after the LED was put in place of the white halogen light, fringes were distinctly visible. However, the LED light was extremely dim compared to the bright halogen light used to take data with the red light filter. For this reason no quantitative data using LEDs were taken.

6 Future Work

There is some work that can be done immediately to improve on the aim of this project – the characterization of broadband sources. First, it is essential to develop a program for Fourier transforming interferogram data. Fourier transforms of data would help to resolve the spectra of the different light sources that are being examined, making the relationship between spectral composition and bandwidth and coherence and visibility properties of light

even clearer.

It would also be beneficial to acquire a superluminescent diode (SLD) for analysis. Not only would it help to examine the most common light source used in OCT, but the mechanisms created and implemented in the course of this study can also be used in conjunction with an SLD to create an open-air OCT setup. Open-air setups are possible, albeit somewhat problematic, to build. There are research groups that have created open-air setups, although most now use fiber optics [5]. The physical components used in a future OCT arrangement would essentially be the same as those in use now.

The two current systems of translation can be used in conjunction in an OCT system. By using the lever as the reference arm depth selector and then moving the mirror back and forth in tiny steps with the rubber band to create the AC signal, the goal of creating a simple one-dimensional OCT device can be realized.

7 Conclusion

In exploring the properties and behavior of various high- and low-coherence light sources, two novel translation methods capable of nanometer-scale resolution, elastic based and lever based translation, were developed and implemented. Fringe patterns resolved using both methods were of high enough resolution to be Fourier transformed, although a different approach was taken in determining spectral bandwidth of the examined light sources by measuring visibility.

Use of a high-coherence He-Ne laser tested the consistency of the scanning devices; coarse measurements taken with the visibility of a sodium gas lamp interference curve then yielded an accurate measurement of the sodium doublet separation; finally, interferogram data taken from a 10 nm bandwidth red light source which mimicked the broadband nature of OCT light sources resulted in a calculation of frequency distribution with very low error. With all light sources observed, a running comparison of frequency spread and coherence length was kept to further illustrate the inverse relationship between these two characteristics of light.

Concepts central to OCT such as the need for high bandwidth, low coherence sources for high scanning resolution and the requirement for instruments which are precise and stable have been addressed throughout the experiment. Great emphasis was placed on creating a more effective scanning Michelson interferometer for the purposes of developing a better setup in the field of OCT, a technique which has numerous benefits in medical diagnostics.

References

[1] "Coherence Physics." http://coherence-physics.wikiverse.org/

[2] D. Huang, E. A. Swanson, C. P. Lin, J. S. Schuman, W. G. Stinson, W. Chang, M. R. Hee, T. Flotte, K. Gregory, C. A. Puliafito, and J. G. Fujimoto. "Optical coherence tomography." Science 254, 1178-1181 (1991)

[3] Scott E. Fraser et al. "An optical coherence microscope for 3-dimensional imaging in developmental biology." Optical Coherence Microscopy Group at Harvey Mudd College.

[4] Mark E. Brezinski and James G. Fujimoto. "Optical Coherence Tomography: High-Resolution Imaging in Nontransparent Tissue." IEEE J. Select. Topics in Quantum Electron, vol. 5, pp. 1185-1191, 1999.

[5] Laboratory of Dr. Yingtian Pan, Stony Brook University.
http://www.bme.sunysb.edu/bme/people/faculty/

[6] Amir H. Nejadmalayeri. "Optical Coherence Tomography." University of Toronto.

[7] Joseph M. Schmitt. "Optical Coherence Tomography (OCT): A Review." IEEE J. Select. Topics in Quantum Electron, vol. 5, pp. 1205-1215, 1999.

[8] Eric Sztanko. "Imaging Fourier Transform Spectrometer."
Center for Imaging Science, Rochester Institute of Technology.
http://www.cis.rit.edu/research/thesis/bs/2001/sztanko/toc.html

[9] Vladimir Shidlovski. "Superluminescent Diodes. Short overview of device operation principles and performance parameters." SuperlumDiodes Ltd.

[10] Eric W. Weisstein. "Fourier Transform Spectrometer."
http://scienceworld.wolfram.com/physics/FourierTransformSpectrometer.html

[11] Jacques Charrier. "Michelson's Interferometre."
http://www.sciences.univ-nantes.fr/physique/enseignement/english/michp.html

[12] Donald K. Berkey and Allen L. King. "An Undergraduate Experiment in Fourier-Transform Spectroscopy." Am. J. Phys., vol. 40, pp. 267-270, 1972.

[13] Robert John Bell. Introductory Fourier Transform Spectroscopy, Academic Press, 1972.

[14] J.C. Albergotti. "Fourier Transform Spectroscopy Using a Michelson Interferometer." Am. J. Phys. 40 (8), 1070-1078 (1972)

[15] Frank L. Pedrotti, Leno S. Pedrotti. Introduction to Optics, Prentice Hall, 1993.

[16] Robert C. Weast and Melvin J. Astle. Handbook of Chemistry and Physics, Chemical Rubber Press, 1981.